Silicon (2022) 14:3269–3280
https://doi.org/10.1007/s12633-021-01058-8

ORIGINAL PAPER

Different Electrode Configurations for NH_3 Gas Sensing Based on Macro Porous Silicon Layer

Ali A. Yousif[1] · Husam R. Abed[2] · Alwan M. Alwan[3]

Received: 12 December 2020 / Accepted: 8 March 2021 / Published online: 15 April 2021
© Springer Nature B.V. 2021

Abstract
In this work, macro porous silicon layers were fabricated by Laser Assisted Etching. The morphology, structure and luminescence characteristics of the porous Si were examined as functions of the etching time using Field Emission-Scanning Electron Microscopy (FE-SEM), Atomic Force Microscopy (AFM) and Photoluminescence (PL). FE-SEM pictures revealed that the macro porous silicon surface layer has macro pores with a similar structure, also the thickness of this layer and the average pore diameter have increased with the increase of etching time. The specific surface area was measured by BET method and it was found in range of 152–213 m^2/g. The AFM images manifested the high roughness and root mean square at low current density which can affect the porous silicon for the gas sensing applications. The PL spectra gave the luminescence energy in the orange–red region of the visible spectrum with the energy band gap of around (2.01 eV) for n-Si etched for 16 min. Two electrode configurations have been investigated for the sensing performance toward the NH_3 gas; planar and sandwich, the former depicted a gas response of 1.85, while the latter revealed an efficient and ultra-gas response of 3.5 with the fast response and recovery times.

Keywords Porous silicon · Laser assisted etching · Gas sensor · NH_3 · Photoluminescence

1 Introduction

One of the main sources of contamination is the toxic ammonia gas molecules generally emitted due to the decomposition of the nitrogenous organic from animals and plant materials, motor vehicles and the excesses of industries [1]. Moreover, the significant chemicals manufacturing was used to produce fertilizers, cleaning products, treatments, explosives, and artificial fibers. Nevertheless, the toxic gas ammonia is a harmful matter and could cause swelling and burn in the air route, skin and eye destruction, and lung impairment. Thus, the sensor for ammonia gas molecules designed with a huge sensitivity, fast response, and extended constancy is critical and immediately required. With the purpose of understanding the detection of NH_3 at the room temperature, researchers have conducted many works and studied a variety of sensitive materials [2–5]. Porous silicon (PS) offers great potential applications as gas sensor devices working at the room temperature because of their amazing feature; high specific surface area. Also, it has been reported that the presence of O_2, NH_3, CO_2, NO_2 gases and many other molecules can alter the conductivity of PS layer [6–8]. It is observed that the macro porous silicon with the pores of micron size could be exposed to the surroundings [9], which elevates the diffusion of the gas considerably. Nevertheless, the specific surface obviously decreased and then affected the gas sensor response, when compared to the nano and meso sized PS of branchy pore channels. Consequently, the specific intermediate PS microstructure with the specific surface area is higher than the micron sized of macro PS, and the gas diffusion channels are more than meso-PS. Therefore, the advantages of meso PS and macro PS can be combined by the intermediate PS [10]. The fabrication of porous silicon by laser-assisted etching method provides a uniform distribution of pores with a large diameter and a high surface area [11]. Furthermore, the low cost,

✉ Husam R. Abed
hussamrafat@yahoo.com

[1] College of Education, Mustansiriyah University, Baghdad, Iraq

[2] The General Directorate of Education in the province of Baghdad - Rusafa /2, Ministry of Education, Baghdad, Iraq

[3] Department of Applied Sciences, University of Technology, Baghdad, Iraq

simplicity of set-up, and ease of controlling pore size by changing the etching conditions made the laser-assisted etching method preferable and highly efficient [12]. Kayahan [13] prepared porous silicon by electrochemical etching method and found that the pores have a diameter of about 2–3 µm. However, a planar configuration for the gas detection characteristics was used. Selvakumar and Sujatha [14] fabricated macro porous silicon by electrochemical etching process using 50 % of HF concentration and found that the macro pores are in the range (0.95-5 µm), also the thickness of the pore is about 4 µm. A planar contact configuration for the gas sensing performance was utilized. Yan and et al. [15] synthesized macro porous silicon by electrochemical etching process at a constant current density of100 mA/cm^2. It was found that the porous silicon has a diameter of about 1.5 µm. After that, a platinum electrode was deposited on the top of the sample for the chemical sensing application. Most of the recent works have focused on the electrochemical etching process for the porous silicon fabrication, and a lot of them deposited the electrode on the top surface of the sample only. This paper is related to the investigation of the sensing performance to NH_3 target gas based on a different electrode configurations. Moreover, this work seeks to reach the high surface area of porous network and large pore diameter which will improve the adsorption rate and hence obtain an effective sensor device. This study aims to fabricate macro porous silicon by laser-assisted etching process depending on the high laser wavelength and the constant current density. Later, the parameters of the porous silicon layer, such as porosity, thickness, specific surface area, and the enhanced morphology and topography, which are optimized to test the different configurations of the NH_3 gas sensing, are experimentally investigated and demonstrated the best way of electrode connection for ultra-gas response.

2 Experimental Part

The n-type silicon wafer with the characteristics of 10 Ω.cm of resistivity and (100) direction of the orientation was used to fabricate the macro porous silicon layer by exploiting the laser-assisted etching technique for this purpose. A simple process of removing the oxide layer from the silicon wafer was done before the etching procedure [16], this process was successfully conducted by dipping the silicon samples after cutting them into 2 × 2 cm^2 for each sample in a solution of Hydrofluoric acid (10 % concentration) for 7 min. The optimum conditions for the fabrication of macro porous silicon layer were obtained with the best duty by utilizing the etching solution with a concentration of (1:1) (40 % of Hydrofluoric acid: Ethanol absolute of 99.999 purity). The etching process was carried out under the circumstance of a current density fixed at the value of (12 mA/cm^2) supplied for the samples for diverse etching durations (4, 8, 12, and 16 min) under a laser illumination of intensity 30 mW/cm^2 and 642 nm wavelength. Subsequently, the porous silicon was rinsed in deionized fine H_2O, and then the samples were exposed toward the ambient air for 2 min. Figure 1 illustrates the experimental setup of the laser-assisted etching process.

3 Methodology

As revealed in Fig. 1, the system of laser-assisted etching consists of Teflon cell, aluminum electrode, electrolyte solution, platinum electrode (provide electrons to electrical circuit), power supply, ammeter, and laser source. After the cleaning process of silicon wafer was completed, the wafer was put on the aluminum substrate inside the Teflon cell within the electrolyte solution. Afterward, the laser source was positioned in a straight direction to the silicon wafer at a distance of 25 cm, which covered 1.5 cm^2 of the sample. At the moment that the samples are put within the solution, the Si-H bonds are established. Next, the power supply was turned on and let the charge carriers to move in the electrical circuit, with the presence of a large amount of holes that came from the induced electron-hole pair generation by laser beam, and the fluoride ion will attack the Si-H bond on the surface of the sample. From this process, a hydrogen atom will release. Later, another fluoride ion will attack the same Si-H bond, resulting in liberating H_2 molecule which can be observed as bubbles in the solution. After this process, the Si-F bond first formed and then was attacked by another fluoride ion leading

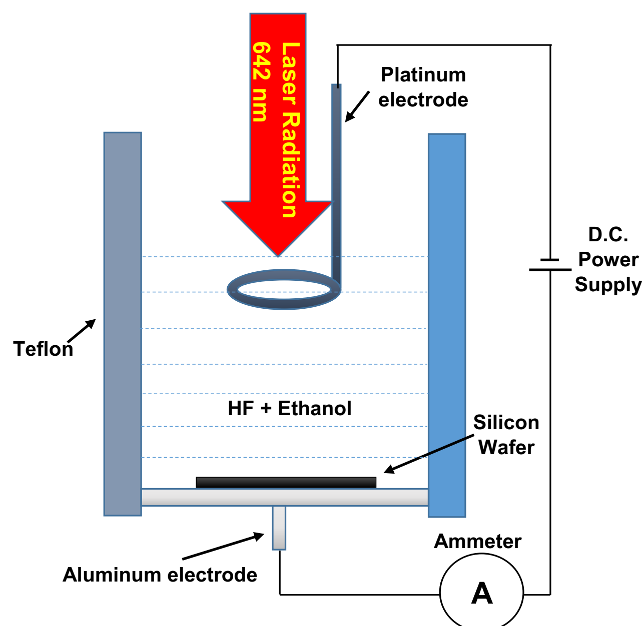

Fig. 1 Schematic diagram of etching system with illumination source

to eliminate of the silicon atom from the surface. The laser source in this route will provide a lot of holes to be reacted with the fluoride ions and hence increasing the snatched silicon atoms. Also, the laser source with a certain wavelength will help use the low current density and the short etching time, this will lead not to reach the electropolishing state.

4 Characterization

The surface morphology of the films was investigated by field emission scanning electron microscopy (INSPECT-550) and atomic force microscope (CSP model AA3000 AFM supplied by Angstrom Company) for the topography of surface, while the photoluminescence spectra were obtained at the room temperature with a Hitachi 3100 spectrophotometer. The sensing route characteristics were successfully completed in a system, including a chamber made of glass, a digital multimeter, and a computer for gaining the data. Two types of electrodes' configurations were deposited on the sample; planar and sandwich, as illustrated in Fig. 2. In planar configuration, the aluminum (Al) electrodes were deposited on the film surface with the dimensions of 2 mm width, 4 mm length, and 25 nm thickness, while in a sandwich configuration, the Al electrodes were deposited on both the top and bottom (50 nm thickness) film surface. The aluminum electrode was deposited by Chemical Vapor Deposition (CVD). When the target gas (ammonia) presents into the chamber, the digital multimeter records the variation in the resistance value for both planar and sandwich configurations continuously. The gas concentrations were well controlled by diluting the standard gas. The response time and the recovery time were determined utilizing the time required to reach 90 % of the total resistance variation. The sensing of the ammonia gas molecules was measured at the room temperature (26^oC) with a relative humidity of (32 %) at a fixed bias voltage of (5 V).

5 Results and Discussion

The controlling parameters of the porous silicon samples layer are based mainly on the layer thickness (d) and the porosity (P%). The values of these two parameters were estimated by the gravimetric method according to the following formulas [17, 18]:

$$P = (\text{Mass }1 - \text{Mass }2)/(\text{Mass }1 - \text{Mass }3) \quad (1)$$

$$d = (\text{Mass }1 - \text{Mass }3)/(\rho \times A) \quad (2)$$

Where, Mass 1 and Mass 2 are the mass of the macro porous silicon sample before and after the etching process, respectively. Mass 3 is the mass measured after eliminating the porous layer, ρ is the density of Si (g/cm^3), and A is the area of the macro porous silicon layer (cm^2). Mass 2 and Mass 3 were determined for the dried samples in vacuum system. The porosity as a function of etching time and the layer thickness versus the etching time are demonstrated in Fig. 3. It is clear from Fig. 3a that the porosity is raising semi-linearly with the increasing of etching time, and the highest value is 76 % at 16 min of etching duration. The thickness of the porous layer was observed to be growing with the increasing of etching time, as evinced in Fig. 3b, and the highest value for the layer thickness is (4.52 μm) at the etching time of 16 min. The amounts of layer thickness and porosity were estimated with the error bars of about (± 5 %).

The macro porous silicon having a thick layer makes the sensor more suitable and very active for the adsorption of gas molecules [19]. The porosity and thickness of porous silicon

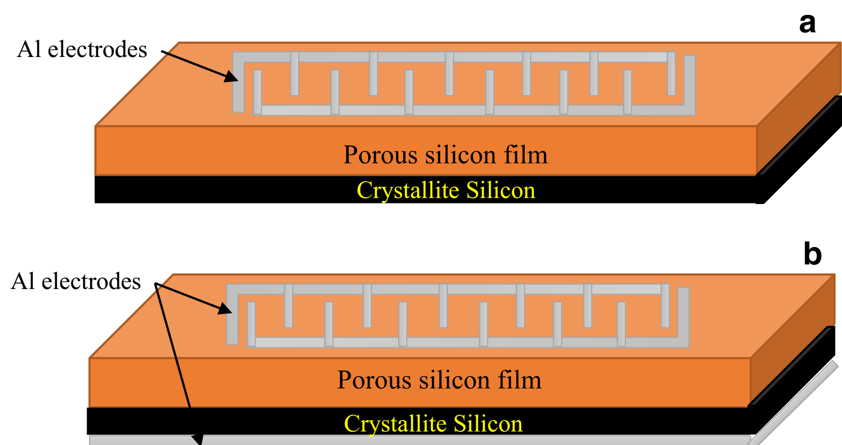

Fig. 2 Schematic of (**a**) planar and (**b**) sandwich electrodes

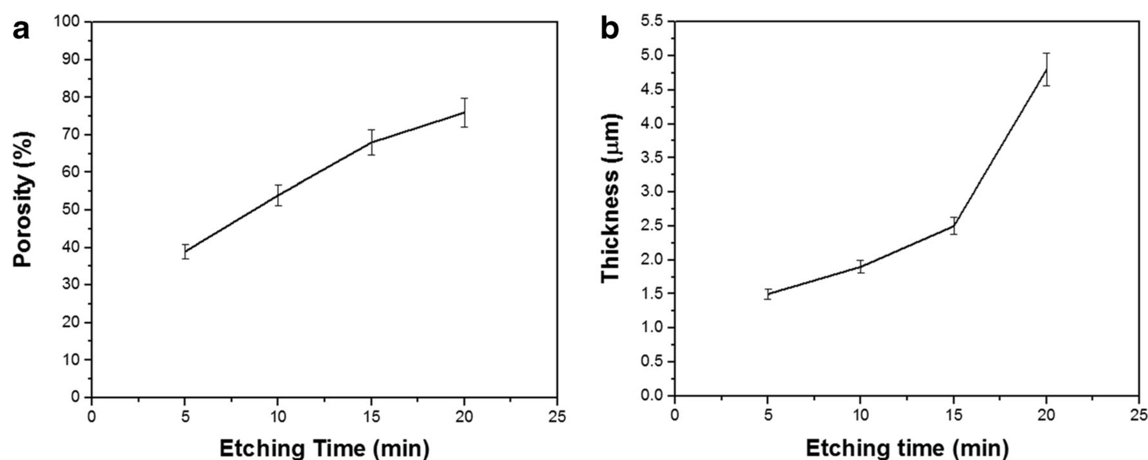

Fig. 3 **a** Porosity versus etching time and **b** Thickness versus etching time

are the most important factors that could affect the gas sensing performance. The porosity increases linearly with the increasing of etching time; this is because of the regular generation of pores along the etching duration and the regular distribution of pores along the silicon matrix. The porous silicon thickness increases exponentially with the increasing of etching time which is related to the large amount of branched pores that contribute to increasing the thickness of porous silicon [20], also it is related to the path of the current inside the pore, and hence depending on the carrier concentration inside the pore. The porous layer thickness is related to the absorption coefficient and its value of about the reciprocal to the absorption coefficient. The absorption coefficient of porous layer decreased with the decreasing of the silicon nanocrystallite sizes due to the increase of the energy gap of the porous silicon layer.

BET method was used to find the specific surface area and diameter of the pore. Furthermore, from this technique, one can obtain the type of the pore shape, whether it is nanoporous, mesoporous, or macroporous. Figure 4 reveals the specific area and diameter of the pore measured by BET method based on the adsorption and desorption rates of the N_2 gas molecules by porous silicon layer. The hysteresis loop is clear in Fig. 4 which is attributed to the partial condensation process that happened inside the macropores. As known that the adsorption process is opposite to the desorption process, however, the evaporation from the macro pores occurs usually at a lower pressure than that of capillary condensation results in the hysteresis loop [21]. In the hysteresis case, the desorption rate is lower than the adsorption rate. The condensation of the gas molecules inside the pores is related to the reduction of the thermal conductivity of porous silicon, and hence increasing the pressure of the molecules inside the pores. The type of hysteresis loop that manifested in Fig. 4 is H3 which is related to the large distribution of pores along the porous matrix, as classified by the International Union of Pure and Applied Chemistry (IUPAC) [22]. This figure depicts that the specific surface area of PS samples increased from (152 m^2/g) to (213 m^2/g) with the increase of etching time from (4 min) to (16 min), respectively. Moreover, the inset figures determine the pore diameter of PS samples, and it is found that the peaks of the pore diameter are (1.5, 1.6, 2.05, and 2.4 μm) corresponding to different etching times (4, 8, 12, and 16 min), respectively. The increase in the values of surface area leads to an enhancement of the surface to adsorb more target gas molecules; this is due to the augmentation in pore diameter which confirms the macro porous type.

The surface morphology characteristics of the porous silicon layer, such as pore-like structure, width of the pores, and wall thickness between the nearby pores are intensely dependent on the etching process factors, specifically the illumination wavelength and the etching period. These characteristics of macro porous silicon have been inspected by direct imaging of the surface morphology structure utilizing FE-SEM. Figure 5 manifests the morphological images for the surface layer of the macro porous silicon samples prepared by laser-assisted etching at (40 mW/cm^2) laser intensity and four etching times (4, 8, 12, and 16) min. The surface morphology of porous silicon in Fig. 5a depicts that the surface structure has a rectangular and irregular pores shape; this is because of the overlapping of the adjacent pores, and the randomly distributed pores on the surface of crystalline silicon. The reason behind the pores overlapping is attributed to the extreme etching process at a high intensity of laser illumination [23]. The pore diameters of the macro porous silicon increase with the increasing of etching time, since the pore sizes have a range of about (0.14–2.52) μm at an etching time of 4 min, (0.18–3.4) μm for etching time 8 min, (0.35–4.45) μm at etching time of 12 min, and about (0.58–5.65) μm at an etching time of 16 min, as elucidated in Fig. 5b-d. The sizes of the pores demonstrated that the macro porous silicon layer was fabricated. This distribution was almost asymmetrical due to Gaussian distribution for the laser beam, where the laser intensity at the center is larger than at

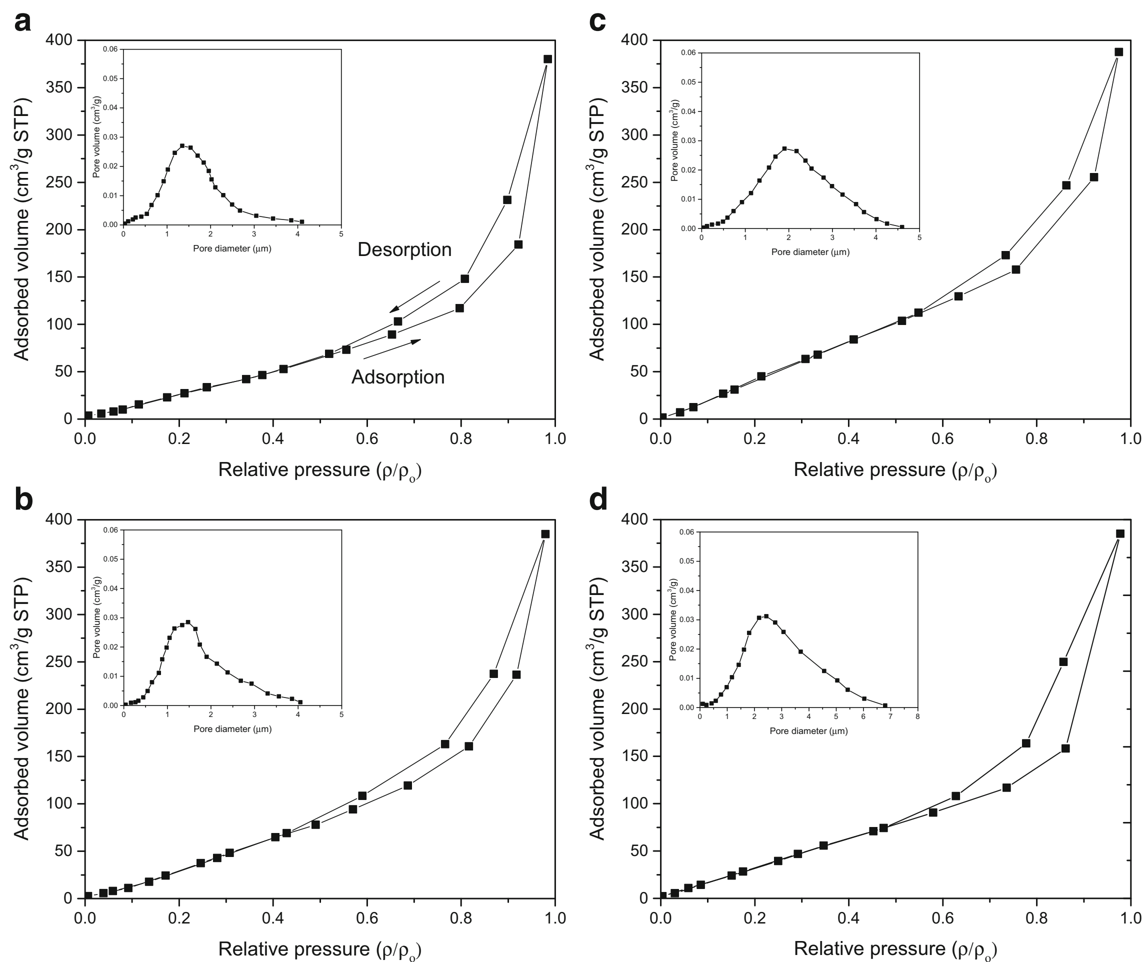

Fig. 4 BET analysis of the adsorbed volume versus relative pressure, and the inset figures are the pore volume versus pore diameter for porous silicon synthesized with different etching times: (**a**) 4 min, (**b**) 8 min, (**c**) 12 min, and (**d**) 16 min

the edge [24]. The cross-sectional images display the increase in the depth of pores as the etching time is increased.

AFM images of PS organized on the n-type silicon wafer and etched with different etching times and (12 mA/cm^2) current density give the formation of uniform PS structures on the Si wafer. The average roughness and the root mean square have been estimated and listed in Table 1. Figure 6 views the 2D and 3D AFM images for n-PS. The surface topography of the n-PS layer fabricated by the AFM analyses is shown homogeneous and without any crack. The high values of RMS and roughness are at 16 min; these values will increase and improve the adsorption rate between the porous layer and the gas molecules.

All the samples of porous silicon evince visible PL at the room temperature. Figure 7 demonstrates the PL spectra at the room temperature for the n-type samples with different formation times: 4, 8, 12, and 16 min. The excitation was induced by the wave of 325 nm. It is clear from the figure that there is a blue shift, which means that as the etching time increases, the energy band gap increases and hence the silicon nano size decreases, this can be attributed to the increasing of pores diameter, Lin et al. [25] and Behzad et al. found the same behavior [26]. Table 2 lists the energy band gap and the silicon nano size (L), the energy band gap is related to the silicon nano size according to this equation [27]:

$$E_{g(PS)} = E_{g(S)} + 88.34/L^{1.37} \tag{3}$$

Where, $E_{g(PS)}$ is the energy band gap of the porous silicon, $E_{g(S)}$ is the energy band gap of the bulk silicon, and L is the silicon nano size.

Two different configurations for gas sensing are discussed here; the first one is the planar configuration (Al/PS/n-Si), in which the electrodes deposited only on the surface of the film. A variation in the resistance of PS sensors with the time for different concentrations of gas was verified, as illustrated in Fig. 8a-d at the room temperature. All the curves in this figure reveal that as the time increases, the resistance of thick film decreases rapidly with the time as the sample is exposed to the ammonia gas molecules. Later, the resistance comes to be saturated, but when the pipe of the chamber is opened, it will give the chance for the ammonia gas molecules to exit, the measured resistance raised and reached to its initial value. The

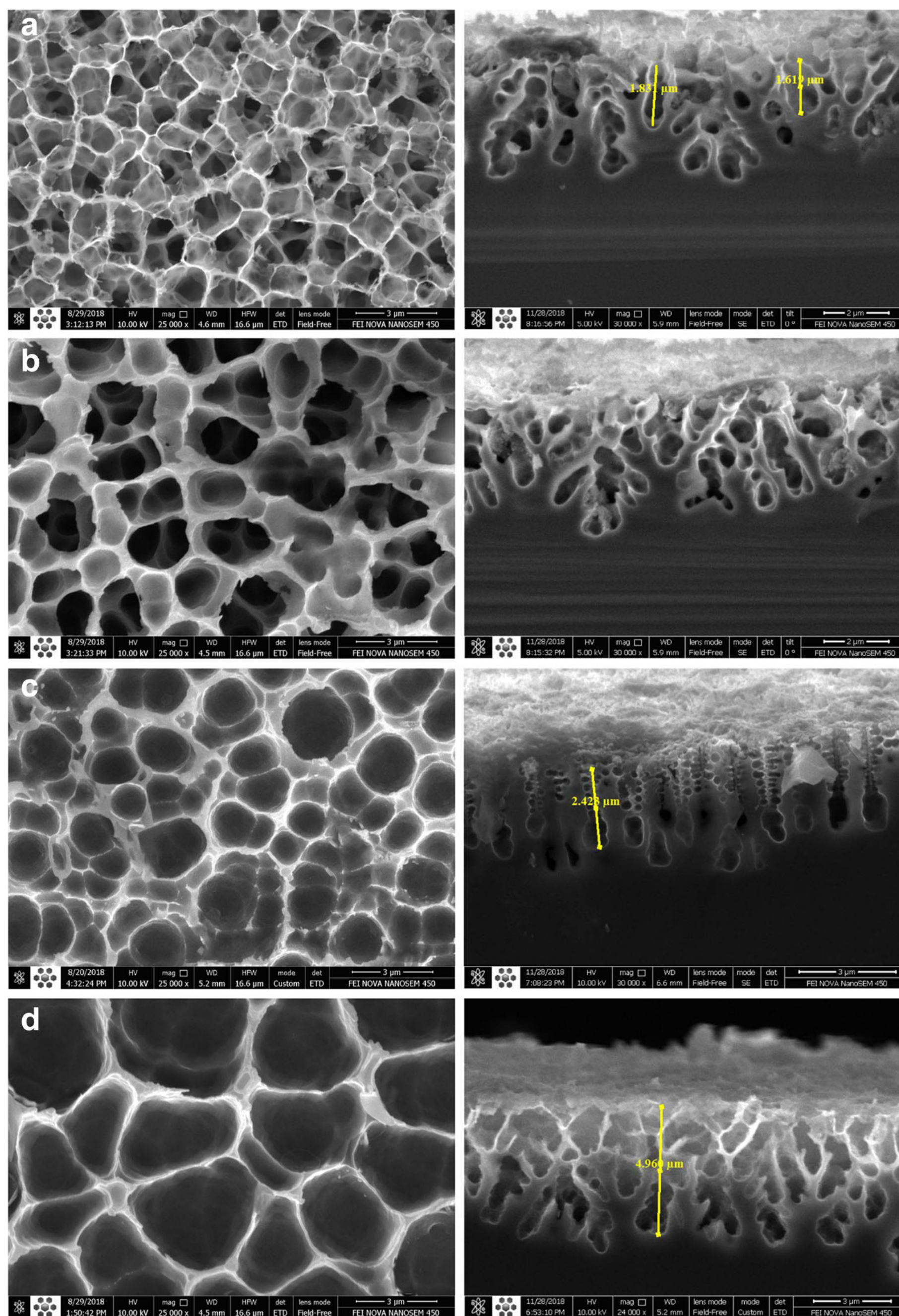

Fig. 5 FE-SEM images with the cross-sectional images of porous silicon for different etching times: **a** 4 min., **b** 8 min., **c** 12 min. and **d** 16 min

resistance of porous silicon displays a reduction from the major value to the minor value, and the statistical value of resistance is changed conforming to the etching duration of n-type silicon. Also, from this figure, it can be noted that the gas response increased when its concentrations are increased. Table 3 depicts the response time, recovery time, and the gas response toward NH_3 gas based on porous silicon at 150 ppm concentration. From this table, it can be seen that as the etching time is growing, the gas response gets boosted and reached to an excellent value of (1.85) at the room temperature. The response time and recovery time reduced with the increasing of etching duration. These values evidenced the best

Table 1 Root mean square and roughness

Sample	Root mean square (nm)	Roughness (nm)
4 min.	16.5	13.3
8 min.	17.1	14.3
12 min.	32	27.4
16 min.	36.9	31.7

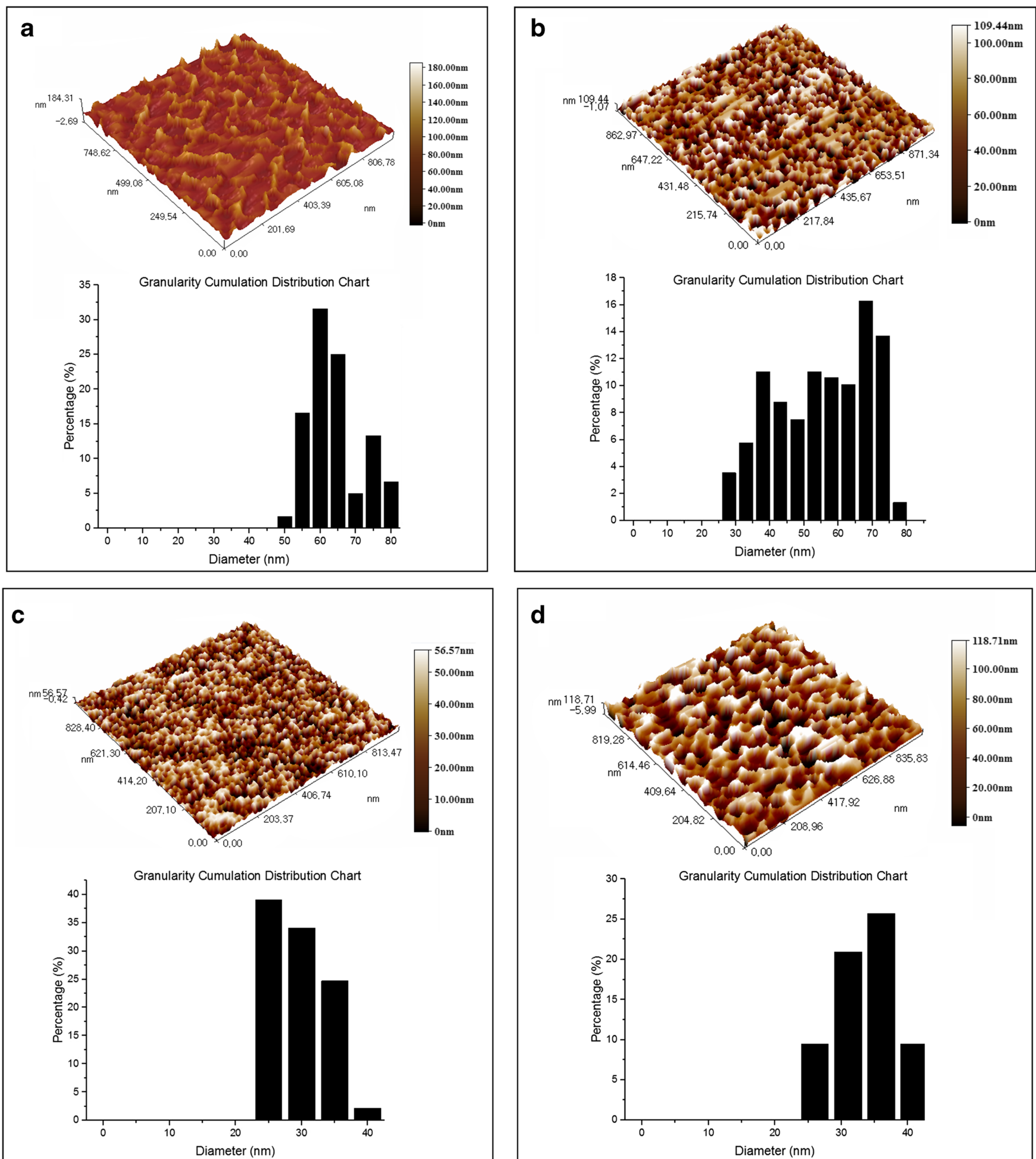

Fig. 6 2D and 3D AFM images of PS for different etching times: **a** 4 min, **b** 8 min, **c** 12 min, and **d** 16 min

sensor device to the ammonia gas molecules at the room temperature. The sensitivity at the lowest gas concentration of 50 ppm is 1.41 for the planar configuration tested at the room temperature which is a good value for detecting the NH_3 gas at the humid air of 32 %. In this case, the flowing of current depends on the channels between the pores of the surface of PS layer. The gas response for this type of configuration was determined by [28]:

$$Gas\ response = \frac{R_a}{R_g} \tag{4}$$

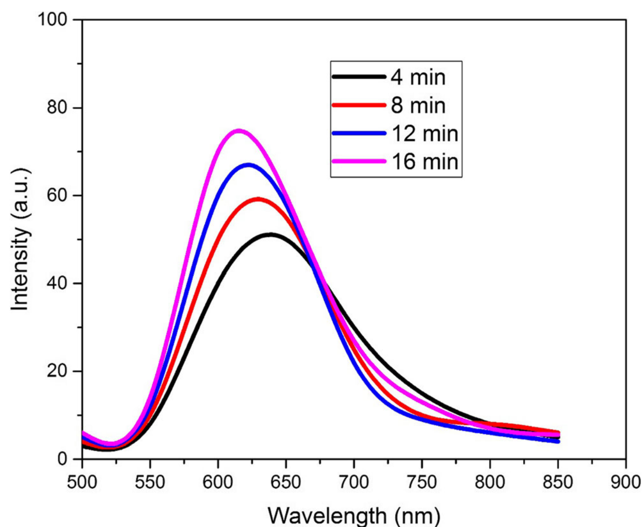

Fig. 7 PL spectra of PS at different etching times

Where, R_g is the measured resistance in the presence of NH_3 gas, and R_a is the resistance that measured in the absence of NH_3 gas.

On the other hand, the second configuration for testing the gas sensor is the sandwich structure (Al/PS/n-Si/Al). The resistance as a function of time for porous silicon sensors is elucidated in Fig. 9a-d, from this figure; it can be observed that the resistance is decreasing with the increasing of gas concentrations.

The response time, recovery time, and the gas response are listed in Table 4 for the sandwich configuration, from this table, it can be noticed that the higher gas response is 3.5 with the fast response and recovery times. Moreover, the sensitivity of sandwich configuration at low concentration of 50 ppm NH_3 gas is 1.85 which is very high compared to the planar configuration. Because of the best values that obtained from this configuration, hence, this is the optimum sensitive device towards the NH_3 target gas at 32 % relative humidity. Therefore, this device could be more effective and reactive to the gas molecules at lower concentration, which can be used in the electronic devices based gas sensor to protect the human from its toxicity and damaging the respiratory system. The reason behind the large value of gas response could be attributed to the

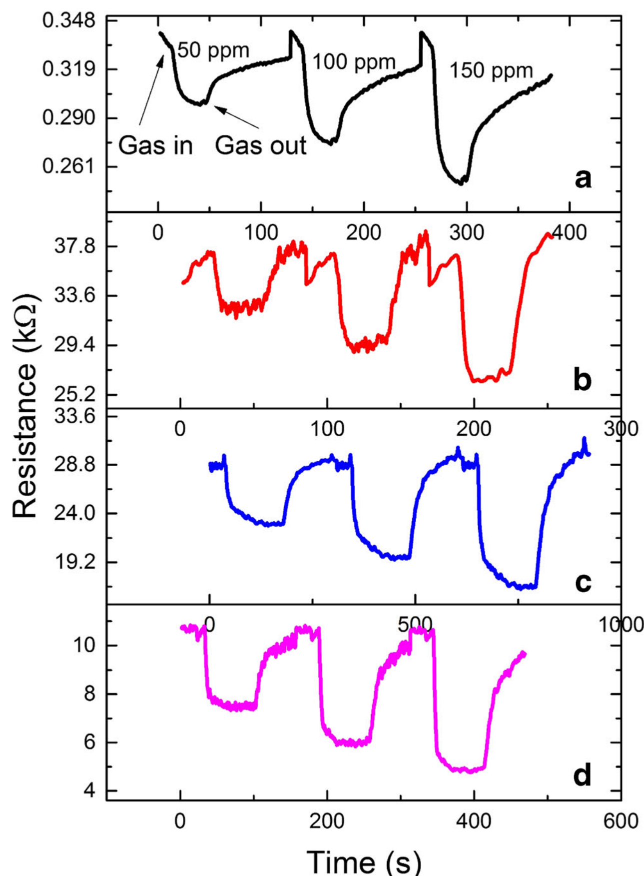

Fig. 8 Resistance-time variation of porous silicon etched for different times: **a** 4 min, **b** 8 min, **c** 12 min, and **d** 16 min

high surface roughness, the optimized morphology of porous silicon, and the high amount of porosity; these make the adsorption rate between the porous layer and the NH_3 gas molecules more effective. In this configuration, the current flow depends on the thickness of pores and the amount of the large diameter pores. Mingda Li et al. [29] found that the response to the NH_3 gas based on porous silicon is 4.5, by utilizing 125 mA/cm^2 current density and 20 min etching time. In another work conducted by Suwan Zhu et al. [30], it was observed that the gas response to the ammonia gas molecules is 1, and the response and recovery times are found less than 25 s and 10 s, respectively. Qin et al. [31] used a porous silicon nanowire array for the gas

Table 2 Energy gap and nano size of PS

Etching time (min)	Wavelength (nm)	Energy gap (eV)	Silicon nanosize (nm)
4	638	1.94	30.44
8	629	1.97	29.65
12	621	1.99	29.15
16	616	2.01	28.67

Table 3 Response time, recovery time, and gas response to 150 ppm of NH_3 gas at the room temperature (planar configuration)

Sample	Response time (s)	Recovery time (s)	Gas response (R_a/R_g)
4 min	33	40	1.2
8 min	27	36	1.36
12 min	15	31	1.6
16 min	10	27	1.85

Table 4 Response time, recovery time, and sensitivity to 150 ppm of NH_3 gas at the room temperature (sandwich configuration)

Sample	Response time (s)	Recovery time (s)	Gas response (R_a/R_g)
4 min	30	20	1.25
8 min	24	17	1.4
12 min	16	15	1.62
16 min	8	12	3.5

sensing fabrication and employed p-type silicon to create a porous silicon nanowire by metal-assisted chemical etching for 90 min, and it was found that the gas response towards 100 ppm ammonia gas is around 1 at the room temperature. In comparison with this work, the current density is 12 mA/cm^2 during 16 min for the porous silicon conditions, and it can be noted that the response and recovery times and the gas response recorded excellent values. The huge value of gas response is also related to the high surface area of the porous silicon layer [32]. However, the porous structure supplies a huge site for the adsorption target gas molecules [33, 34]. Additionally, the gas response increases with

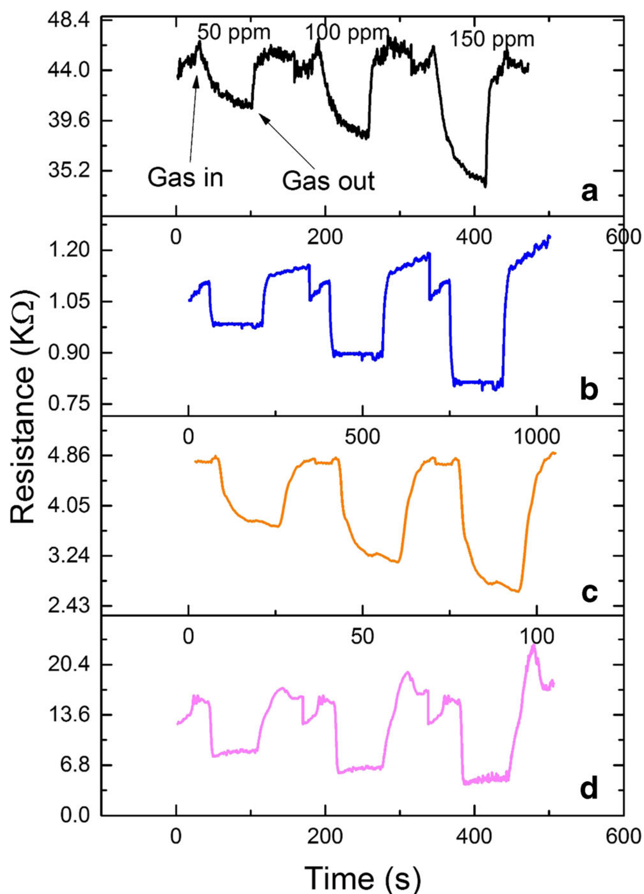

Fig. 9 Resistance as a function of time of PS at different etching times: **a** 4 min, **b** 8 min, **c** 12 min, and **d** 16 min

the increase of gas concentration, proposing that this sensor has the ability to detect the diverse concentrations of target gas. Finally, it should be mentioned that all the samples were checked three times to ensure the value of gas response. Table 5 summarizes a comparison with the previous researches based on the porous silicon ammonia gas sensor.

The sensing mechanism towards the NH_3 gas molecules depends on the morphology, wavelength of laser source, specific surface area of porous network, diameter, and thickness of the pores [43]. When the macroPS exposed to the air, the molecules of oxygen will adsorb the surface of PS resulting in trapping the electrons of conduction band and leading to the decreasing of conductivity, hence increasing the resistance value by transforming the oxygen molecules into chemisorbed oxygen (O_2^-). After the sample exposure to NH_3 gas, the macroPS will adsorb the target gas on the surface and react with the chemisorbed oxygen giving rise to liberate the trapped electrons; this is due to the fact that the NH_3 gas is a reducing gas. This process will decrease the resistivity, and a high variation will occur in the resistance value, hence a large value of sensitivity will be obtained. The reason behind the highest sensitivity towards the target gas is related to the macroPS that has a large pore diameter and an optimum pore thickness obtained by controlling the etching time and specific laser wavelength. Also, the laser source (specific wavelength) will make an increment in the pore diameter, leading to adsorb more gas molecules into pores. Furthermore, the configuration of electrode is a very important factor that specifies the current flow and therefore specifies the value of sensitivity. Because of obtaining the high pore diameter, and the optimum column thickness, the sensitivity to the target gas improved in the sandwich configuration of electrode which depends on the pore size and pore thickness.

6 Conclusion

In this work, an efficient porous silicon layer was successfully fabricated by laser-assisted etching. The used

Table 5 Comparison with the previous works based on porous silicon NH_3 gas sensor

Sensor	Electrode configuration	Source wavelength (nm)	Humidity (%)	Gas concentration (ppm)	Temperature (°C)	Response time (s)	Recovery time (s)	Formula	Sensitivity	Ref.
Black silicon	Planar	515	40–50	100	RT	10 for gas concentration>200 ppm	-	I_g/I_a	1.8	[35]
Silicon nanowire	Planar	Without	-	10	RT	-	-	$(R_g-R_a)/R_a$	0.5	[36]
PS/WO_3	Planar	Without	30	100	RT	-	-	R_a/R_g	3.5	[37]
PS/CdSe nanorod	Planar	Without	29	100	RT	-	-	R_a/R_g	1.8	[38]
Silicon	Planar	515	34	50	RT	288	1122	$(I_g-I_a)/I_a$	144%	[39]
Au/ZnO/n-Si	Planar	Without	-	50	150	18	53	$(R_g-R_a)/R_a$	75%	[40]
Au@ZnO/PS	Planar	Without	Dry air	100	RT	-	-	$(I_g-I_a)/I_a$	23%	[41]
PANI/MSSA	Planar	Without	Dry air	90	RT	-	-	$(R_g-R_a)/R_a$	1.65	[42]
Macro porous silicon	Sandwich	642	32	150	RT	8	12	R_a/R_g	3.5	Current research

Where, I_g is the measured current in the presence of target gas, I_a is the measured current in the absence of target gas, R_g is the measured resistance in the existence of gas, R_a is the measured resistance in the absence of gas, PANI is polyanline, and MSSA is the microstructure of silicon array

photon source with a high wavelength and intensity gives a chance for more holes in the silicon structure to react with the fluoride ions. Therefore, a large amount of silicon atoms was eliminated resulting in a wide pore diameter and a high thickness. Moreover, the utilization of a laser source in this work renders this procedure operating at a low current density and short etching time, which made the work low cost, effective, and saving effort. The average pore diameter appears in a good agreement with what expected for a macro porous layer. From FE-SEM microscopy, it can be observed that the increased etching time leads to increase the pore size, but it has almost no effect on the pore shape. The AFM manifested a homogenous surface with a high average roughness. Photoluminescence exhibited the orange-red region of visible spectrum. The energy band gap of porous silicon is 2.01 eV and it is higher than the energy band gap of bulk silicon which is 1.12 eV, this behavior is due to quantum confinement. There are two configurations for the gas sensing performance; in the planar configuration, the current passing through the surface of porous silicon layer is related to the channels of the pores, while in the sandwich configuration, the current that penetrates the silicon wafer depends on the thickness of pores. The performance of the NH_3 gas sensor evinced that the gas response of films with the sandwich electrodes is two times higher than those films with the planar electrodes, and hence the sandwich electrodes are the optimum configuration for gas sensing. Further works will wide-open a unique scene in the field of applied nano sciences.

Supplementary Information The online version contains supplementary material available at https://doi.org/10.1007/s12633-021-01058-8.

Acknowledgements The authors would like to thank University of Technology, Baghdad-Iraq, Mustansiriyah University, Baghdad-Iraq, and University of Tehran, Tehran-Iran, for their support in the present work.

Author Contributions All authors have contributed equally.

Data Availability The data has been attached in separate files.

Declarations

Consent to Participate Not applicable.

Consent to Participate The authors declare that there is no conflict of interest.

Consent for Publication Not applicable.

References

1. Li X, Li X, Li Z, Wang J, Zhang J (2017) WS_2 nanoflakes based selective ammonia sensors at room temperature. Sensors Actuators B Chem 240:273–277
2. Fengyun S, Ming Hu, Peng S, Jie Z, Bo L (2010) NH3 sensing characteristics of nano-WO3 thin films deposited on porous silicon. J Nanosci Nanotechnol 10(11):7739–7742
3. Alwan AM, Abbas RA, Dheyab AB (2018) Study the characteristic of planer and sandwich PSi gas sensor (Comparative Study). Silicon 10(6):2527–2534
4. Triantafyllopoulou R, Illa X, Casals O, Chatzandroulis S, Tsamis C, Romano-Rodriguez A, Morante JR (2008) "Nanostructured oxides on porous silicon microhotplates for NH3 sensing. Microelectron Eng 85(5–6):1116–1119
5. Meng W et al (2017) Mixed-potential type NH_3 sensor based on TiO_2 sensing electrode with a phase transformation effect. Sensors Actuators B Chem 240:962–970
6. Naama S et al (2015) CO2 gas sensor based on silicon nanowires modified with metal nanoparticles. Mater Sci Semicond Process 38: 367–372
7. Pancheri L, Oton CJ, Gaburro Z, Soncini G, Pavesi L (2003) Very sensitive porous silicon NO_2 sensor. Sensors Actuators B Chem 89(3):237–239
8. Lewis SE, DeBoer JR, Gole JL, Hesketh PJ (2005) Sensitive, selective, and analytical improvements to a porous silicon gas sensor. Sensors Actuators B Chem 110(1):54–65
9. Ouyang H, Christophersen M, Fauchet PM (2005) Enhanced control of porous silicon morphology from macropore to mesopore formation. Phys status solidi 202(8):1396–1401
10. Harraz FA, El-Sheikh SM, Sakka T, Ogata YH (2008) Cylindrical pore arrays in silicon with intermediate nano-sizes: a template for nanofabrication and multilayer applications. Electrochim Acta 53(22):6444–6451
11. Yousif AA, Alwan M, Alwan, Abed HR (2020) Optimizing of macro porous silicon morphology for creation of SnO2/CuO nanoparticles. AIP Conference Proceedings. vol 2213. No. 1. AIP Publishing LLC, Melville
12. Alwan AM, Abed HR, Yousif AA (2020) Effect of the deposition temperature on ammonia gas sensing based on SnO 2/porous silicon. Plasmonics: 1–9
13. Kayahan E (2018) Porous silicon based CO2 sensors with high sensitivity. Optik 164: 271–276
14. Selvakumar VS, Sujatha L (2020) Fast response and recovery of nano-porous silicon based gas sensor. Microsyst Technol 26(3): 823–834
15. Yan D et al (2021) Electrophoretic deposition of multiwalled carbon nanotubes onto porous silicon with enhanced NO2-sensing characteristics. Mater Res Bull 134:111109
16. Habubi NF et al (2015) Annealing time effect on nanostructured n-ZnO/p-Si heterojunction photodetector performance. Surf Rev Lett 22(02):1550027
17. Das M, Sarkar D (2016) Morphological and optical properties of n-type porous silicon: effect of etching current density. Bull Mater Sci 39(7):1671–1676
18. Abed HR et al (2020) Efficient, fast response, and low cost sensor for NH 3 gas molecules based on SnO 2: CuO/macroPSi nanocomposites. Appl Phys A 126(11):1–15
19. Peng S et al (2012) Nano-WO3 film modified macro-porous silicon (MPS) gas sensor. J Semicond 33.5:054012
20. Matthias S, Müller F, Gösele U (2005) Controlled nonuniformity in macroporous silicon pore growth. Appl Phys Lett 87(22):224106
21. Chang S-S et al (2009) Mesoporosity as a new parameter for understanding tension stress generation in trees. J Exp Bot 60(11): 3023–3030
22. Cychosz KA et al (2017) Recent advances in the textural characterization of hierarchically structured nanoporous materials. Chem Soc Rev 46(2):389–414
23. Matsumoto A et al (2020) Laser-induced breakdown spectroscopy using a porous silicon substrate produced by metal-assisted etching: microanalysis of a strontium chloride aqueous solution as an example. J Anal At Spectrom 35(10):2239–2247
24. Le H et al (2020) Effects of top-hat laser beam processing and scanning strategies in laser micro-structuring. Micromachines 11.2:221
25. Lin C-H, Lee S-C, Chen Y-F (1994) Morphologies and photoluminescence of porous silicon under different etching and oxidation conditions. J Appl Phys 75(12):7728–7736
26. Behzad K, Yunus WMM, Talib ZA, Zakaria A, Bahrami A (2012) Effect of preparation parameters on physical, thermal and optical properties of n-type porous silicon. Int J Electrochem Sci 7:8266–8275
27. Diwan BD, Dubey VK (2014) Influence of size on effective band gap of silicon nano-wire. Advanced Materials Research, vol 938. Trans Tech Publications Ltd, Bäch
28. Abed HR, Alwan AM, Yousif AA, Habubi NF (2019) Efficient SnO $_2$/CuO/porous silicon nanocomposites structure for NH $_3$ gas sensing by incorporating CuO nanoparticles. Opt Quantum Electron 51(10):333
29. Li M, Hu M, Zeng P, Ma S, Yan W, Qin Y (2013) Effect of etching current density on microstructure and NH_3-sensing properties of porous silicon with intermediate-sized pores. Electrochim Acta 108:167–174
30. Zhu S, Liu X, Zhuang J, Zhao L (2017) A fast room temperature NH_3 sensor based on an Al/p-Si/Al structure with Schottky electrodes. Sensors 17(8):1929
31. Qin Y, Liu Y, Wang Y (2016) Aligned array of porous silicon nanowires for gas-sensing application. ECS J Solid State Sci Technol 5(7):P380–P383
32. Alwan AM, Yousif AA, Abed HR (2019) High sensitivity and fast response at the room temperature of SnO_2: CuO/PSi nanostructures sandwich configuration NH_3 gas sensor. AIP Conf Proc 2190(1): 20086
33. Sun K-M, Song X-Z, Wang X-F, Li X, Tan Z (2020) Annealing temperature-dependent porous $ZnFe_2O_4$ olives derived from bimetallic organic frameworks for high-performance ethanol gas sensing. Mater Chem Phys 241: 122379
34. Karthik TVK, Martinez L, Agarwal V (2018) Porous silicon ZnO/SnO_2 structures for CO_2 detection. J Alloys Compd 731:853–863
35. Liu X-L et al (2018) "Infinite Sensitivity" of black silicon ammonia sensor achieved by optical and electric dual drives. ACS Appl Mater Interfaces 10(5):5061–5071
36. Qin Y et al (2018) Polypyrrole shell (nanoparticles)-functionalized silicon nanowires array with enhanced NH3-sensing response. Sens Actuators B 258:246–254
37. Qiang X et al (2018) Preparation of porous silicon/Pd-loaded WO3 nanowires for enhancement of ammonia sensing properties at room temperature. Mater Sci Semicond Process 79:113–118
38. Laatar F (2020) Synthesis of the PS/CdSeNRs composite for room temperature NO 2 gas sensing. Silicon: 1–8
39. Liu X-L et al (2020) Light-enhanced room-temperature gas sensing performance of femtosecond-laser structured silicon after natural aging. Optics express 28(5):7237–7244
40. Punetha D, Saurabh Kumar P (2019) Ultrasensitive NH 3 gas sensor based on Au/ZnO/n-Si heterojunction Schottky diode. IEEE Trans Electron Devices 66.8:3560–3567
41. Zhou F, Wang Q, Liu W (2016) Au@ ZnO nanostructures on porous silicon for photocatalysis and gas-sensing: the effect of

plasmonic hot-electrons driven by visible-light. Mater Res Express 3:085006

42. Tai H et al (2015) P–P heterojunction sensor of self-assembled polyaniline nano-thin film/microstructure silicon array for NH3 detection. Chem Phys Lett 621:58–64
43. Sun P, Hu M, Li M, Ma S (2012) Microstructure, electrical and gas sensing propertiesof meso-porous silicon and macro-porous silicon. Acta Phys -Chim Sin 28:489

Publisher's Note Springer Nature remains neutral with regard to jurisdictional claims in published maps and institutional affiliations.